Polymer Degradation and Stability 97 (2012) 2481–2486

Contents lists available at SciVerse ScienceDirect

Polymer Degradation and Stability

journal homepage: www.elsevier.com/locate/polydegstab

Polystyrene/molybdenum disulfide and poly(methyl methacrylate)/molybdenum disulfide nanocomposites with enhanced thermal stability

Zvonimir Matusinovic [a], Ruchi Shukla [a], E. Manias [b], Charles G. Hogshead [b], Charles A. Wilkie [a,*]

[a] Department of Chemistry and Fire Retardant Research Facility, Marquette University, P.O. Box 1881, Milwaukee, WI 53201, USA
[b] Department of Materials Science and Engineering, Penn State University, University Park, PA 16802, USA

ARTICLE INFO

Article history:
Received 28 July 2011
Received in revised form
4 January 2012
Accepted 4 January 2012
Available online 15 July 2012

Keywords:
Fire retardancy
Polystyrene
Poly(methyl methacrylate)
Nanocomposites

ABSTRACT

Nano-sized MoS_2 particles have been synthesized and polystyrene (PS) and poly(methyl methacrylate) (PMMA) nanocomposites have been prepared using solution mixing techniques. X-ray diffraction and transmission electron microscopy were used to characterize the morphology of the nanocomposites. Thermal stability and fire properties of nanocomposites were studied by thermogravimetric analysis and cone calorimetry. Mechanical properties were investigated by dynamical mechanical analysis and tensile testing. The PS/MoS_2 nanocomposites showed enhanced thermal stability in comparison to neat polystyrene, as exhibited by the increase of temperature of 50% mass loss point by over 30 °C in the best case. Reduction in the peak heat release rate was observed in all PS/MoS_2 nanocomposites and even more pronounced effects were found in PMMA/MoS_2 nanocomposite.

1. Introduction

Transition metal sulfides, especially molybdenum sulfide (MoS_2), are scientifically and technologically important materials. In recent years, their synthesis attracted ever increasing interest because of their potential applications in the areas of catalysis [1,2], lubrication [3–5], electrochemistry [6,7] as well as in intercalation chemistry where they serve as host materials [8,9]. Intercalation chemistry of metal sulfides was well known already in the 1970s but molybdenum disulfide has attracted scientific interest only in the last two decades.

MoS_2 exists in two crystalline forms, hexagonal and rhombohedral. The hexagonal form is by far the most common, found in commercial ores, but the rhombohedral form has also been found to occur in nature. The hexagonal form is characterized by MoS_2 layers in which the Mo atoms have trigonal prismatic coordination of six sulfur atoms, with two molecules per unit cell. This forms a layered structure consisting of MoS_2 sandwiches held together by relatively weak van der Waals forces. Each MoS_2 sandwich layer is composed of one molybdenum sheet between two sheets of sulfur and the atoms in a sheets form two-dimensional triangular net. The separation between the Mo sheet and S sheet is 1.59 Å and the distance between the Mo sheets of adjacent sandwich layers is 6.15 Å.

The literature reports several investigations in which MoS_2 has been combined with polymers and these studies have been carried out to increase toughness [10], to change the crystallization behavior in poly(phenylene sulfide) [11], for improved tribological properties [12,13] and to improve the thermal stability of i-polypropylene [14].

Over a period of several years, in this laboratory there have been investigations of the effect of a variety of nano-dimensional particles, including montmorillonite, layered double hydroxides and carbon nanotubes, on the fire retardancy of various polymers [15]. In this work, this is now extended to include MoS_2 as a nano-dimensional material.

In this work, dispersible MoS_2 nanoparticles were synthesized by the scale up of a literature procedure [16] using a mixture of the coordinating solvent trioctylphosphine oxide (TOPO) and octadecene as the synthetic medium. PS/MoS_2 and PMMA/MoS_2 nanocomposites were prepared and the thermal and fire properties of the nanocomposites with various amounts of molybdenum disulfide as a filler were investigated.

2. Experimental

2.1. Materials

Trioctylphosphine oxide (TOPO) technical grade, 90%; molybdenum hexacarbonyl ($Mo(CO)_6$), 98%; elemental sulfur (S); 1-octadecene (ODE), technical grade 90%; toluene, ACS reagent 99.5%; methanol, ACS reagent 99.9%; polystyrene (PS), nominal M_w

* Corresponding author.
E-mail address: charles.wilkie@marquette.edu (C.A. Wilkie).

0141-3910/$ – see front matter © 2012 Elsevier Ltd. All rights reserved.
http://dx.doi.org/10.1016/j.polymdegradstab.2012.07.004

192,000; poly(methyl methacrylate) (PMMA), nominal M_w 996,000; and dichloromethane, ACS 99.5%, were used as obtained from Aldrich Chemical.

2.2. Preparation of MoS_2 nanoparticles

MoS_2 nanoparticles were synthesized via reaction of $Mo(CO)_6$ with elemental sulfur in trioctylphosphine oxide at 270 °C using standard air-free techniques [16].

250 g of trioctylphosphine oxide and 15.0 g (56.8 mmol) of molybdenum hexacarbonyl were added to a 1000 ml three necked round bottom flask fitted with a flow control adaptor, a stopper and an air condenser. The system was brought into inert atmosphere by alternatively applying vacuum and flushing with argon three times. Reaction temperature was then increased to 250 °C under an argon atmosphere and the system was maintained at that temperature for 16 h.

The sulfur precursor solution was prepared by dissolving 3.64 g (113 mmol) of elemental sulfur in 75 ml of 1-octadecene at 130 °C under an Ar atmosphere. When a clear solution was obtained, the system was cooled to 60 °C. Then, the temperature of molybdenum-TOPO solution was increased to 270 °C and sulfur solution (maintained at 60 °C) was added drop-wise with a pipette in batches of 5 ml while maintaining the Ar atmosphere in both flasks. After the addition was complete, the reaction temperature was maintained at 270 °C for 48 h to complete the nanoparticle synthesis. The reaction system was then cooled to 60 °C and 60 ml of toluene was injected to the system to prevent solidification of reaction mixture. The dispersion was subsequently cooled to room temperature. The MoS_2 nanoparticles were isolated by adding an excess of methanol (1.5 l) followed by centrifugation; particles were purified by washing with methanol to remove the excess TOPO and then dried in an oven at 70 °C for 16 h. Yield: 12 g (since MoS_2 retains an unknown amount of TOPO, one cannot calculate the % yield).

2.3. Synthesis of PS/MoS_2 and PMMA/MoS_2 nanocomposites

PS/MoS_2 nanocomposites with 1, 5 and 10% of MoS_2 nanoparticles were prepared as follows. First, polystyrene (90 g) was dissolved in dichloromethane (600 ml) using a magnetic stirrer and ultrasonic agitation. Then, a previously prepared stable dispersion of MoS_2 nanoparticles (10 g) in dichloromethane (100 ml), was added to the PS solution and the system was mixed at room temperature for 48 h covered with aluminum foil followed by 4 h of stirring without cover to remove most of the solvent. Then, the viscous PS/MoS_2 solution was transferred to a container and dried at room temperature until most of the solvent evaporated. The remains were finally transferred to a vacuum oven and left at 70 °C overnight.

PMMA/MoS_2 nanocomposite with 10% of MoS_2 loading was prepared using an analogous procedure.

2.4. Characterization

X-ray diffraction measurements (XRD) were performed on a Rigaku, Miniflex II desktop X-ray diffractometer. Data acquisition was performed using a scan speed of 5°/min, at a sampling width of 0.05° from 2° to 65° (2θ). Transmission electron microscopy (TEM) was performed on a JEOL 1200 EXII microscope, equipped with a Tietz F224 digital camera and operated at an accelerating voltage of 80 kV. Sections 50–150 nm thick of the nanocomposites were obtained with a Leica Ultracut UCT microtome, equipped with a diamond knife. The sections were observed under bright field TEM without any heavy metal staining, since there was enough contrast to distinguish the inorganic fillers from the polymer matrix. Thermogravimetric analysis (TGA) was performed on a Netzch TG 209 F1 instrument. Samples were heated from 30 to 700 °C at a scan rate of 10 K/min under inert nitrogen atmosphere at a flow rate of 20 ml/min. Cone calorimeter measurements were performed on an Atlas CONE-2 instrument according to ASTM E 1352 at an incident flux of 50 kW/m [2] using a cone shaped heater. The exhaust flow was set at 24 L/sec. The specimens for cone calorimetry were prepared by the compression molding of the sample (approximately 30 g) into 10 cm × 10 cm square plaques with thickness of 3 mm. Dynamical mechanical analysis (DMA) was performed on a DMA-Q800 TA instrument in air between 30 and 120 °C with heating rate of 3 °C/min. The tensile test was performed on an Instron 5500 series test instrument at room temperature. The crosshead speed was 12.7 mm/min. Specimens for tensile test were prepared with a CS-183MMX Mini Max molder injection machine.

3. Results and discussion

Fig. 1 shows the X-Ray diffraction (XRD) patterns of commercial MoS_2 and the synthesized MoS_2 nanoparticles. It appears that the commercial MoS_2 has strong crystallinity and a layered structure with an interlamellar distance of 6.15 Å (0.615 nm), as seen from the high order diffraction peaks (004), (006) and (008) shown in Fig. 1. This highly crystalline [17] material is very difficult to exfoliate and disperse in polymer matrices without special procedures [18–20]. However, MoS_2, synthesized by the method described above is unambiguously amorphous as shown by the lack of crystalline or high-order basal peaks in the XRD diffractograms and is therefore presumably very dispersible in various polymer matrices. The absence of the (002) reflection at 6.15 Å ($2\theta = 14.5°$) and a broad feature indicating the absence of crystalline long-range order, strongly suggests a large extent of destacking in the synthesized MoS_2. Fig. 2 shows the XRD pattern of PS/MoS_2 nanocomposite with 5% of MoS_2 as compared to the filler itself. The broad MoS_2 diffraction peak at $2\theta = 9.5°$ is still present in the PS nanocomposite, as a low-2θ shoulder in the PS amorphous halo. However, the broad MoS_2 basal peak at $2\theta = 32–38°$ is barely visible in the PS nanocomposite, suggesting some dispersion of the nanoparticles in the PS matrix. The same observations are observed for PMMA/MoS_2 nanocomposites but not shown here.

The composite morphology of the PS/MoS_2 nanocomposites was further studied by TEM analysis. Fig. 3 presents TEM images of PS/

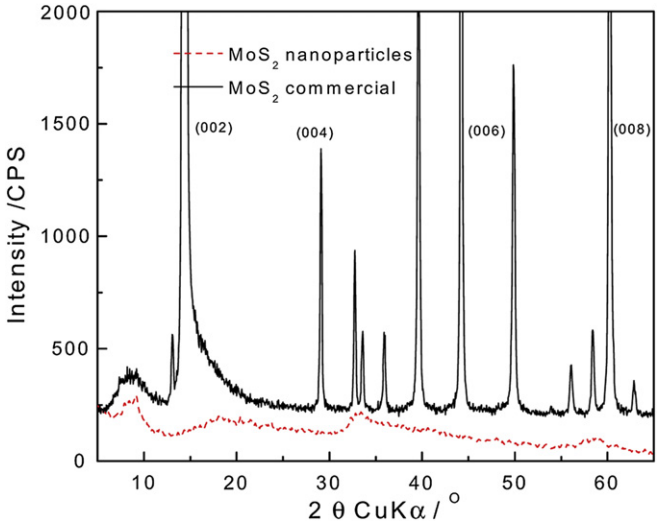

Fig. 1. XRD patterns of commercial MoS_2 and synthesized MoS_2 nanoparticles.

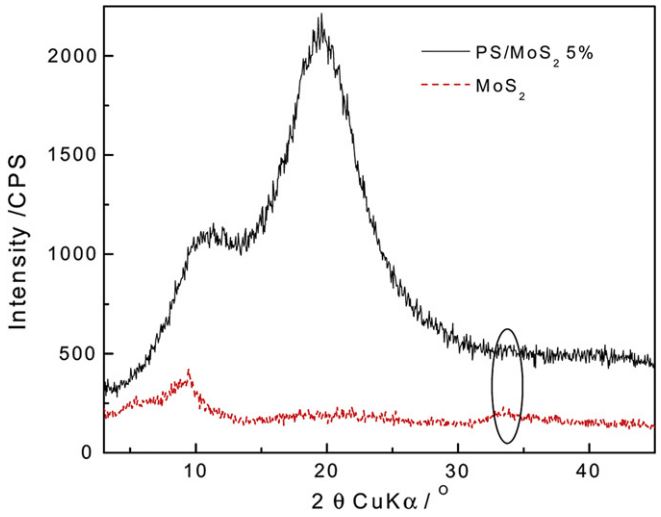

Fig. 2. XRD pattern of PS/MoS_2 nanocomposite with 5% of MoS_2 content in comparison with MoS_2 nanoparticles.

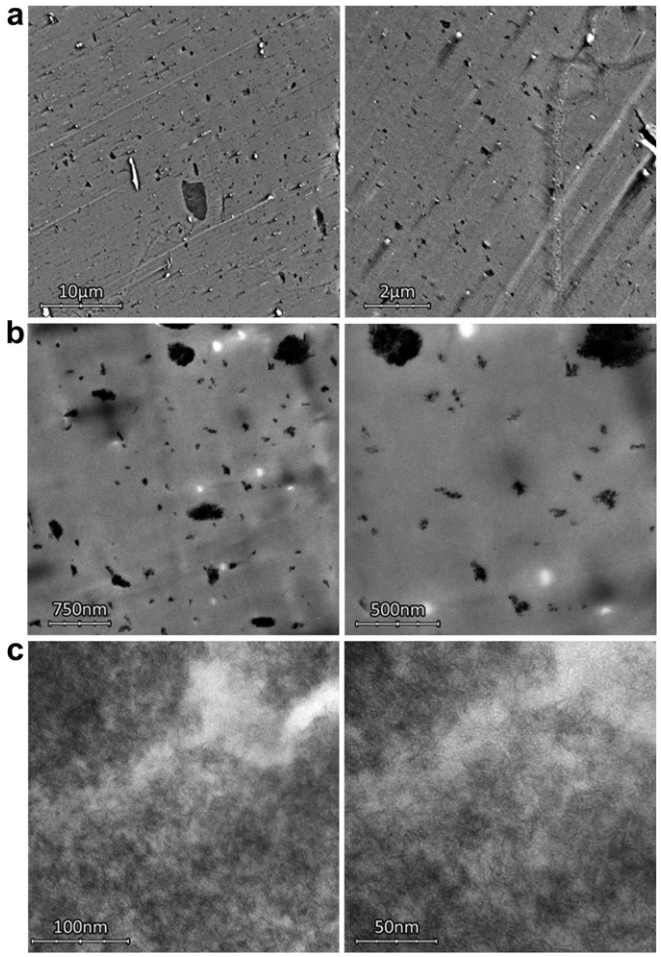

Fig. 3. Bright-field TEM of the PS/10% MoS_2 nanocomposite, demonstrating the hierarchical composite structure over the complete length scale: (a) micron scale structure showing the dispersion of filler clusters/tactoids throughout the polymer matrix. (b) Sub-micron scale structure exemplifying the size and shape of the MoS_2 tactoids; in (b2) it becomes clear that the tactoids are swollen by polymer. (c) nanometer scale structure, specifically imaging the fillers within the biggest tactoids of the composite; at this scale it is clear that the individual filler layers are separated by polymer (dispersed).

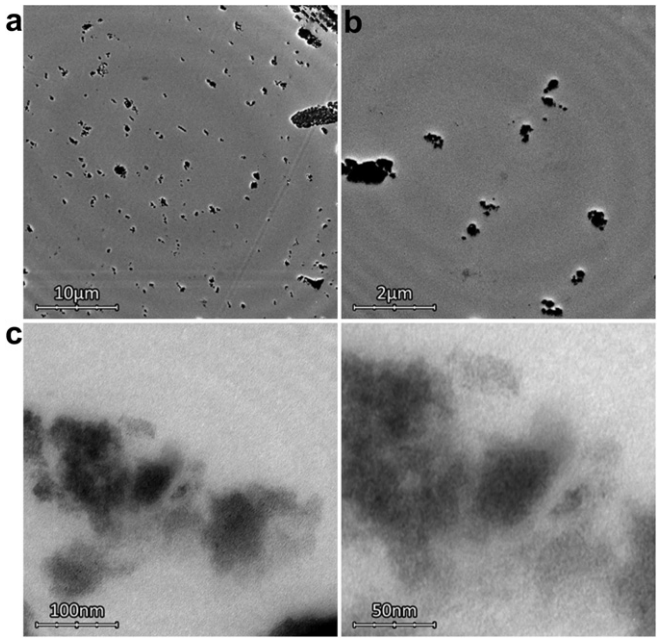

Fig. 4. Bright-field TEM of the PMMA/10% MoS_2 nanocomposite, demonstrating the composite structure. At the micron length scale, and at low magnification (a) the dispersion of filler tactoids in the polymer matrix is shown, whereas at higher magnification (b) the shape and size of the tactoids is demonstrated. At the nanometer scale (c), it is shown that the fillers within the tactoids are swollen by PMMA polymer.

MoS_2 nanocomposites at 10% MoS_2 content, showing representative structures from several micrometers down to the nanometer size features, where individual layers can be resolved. The MoS_2 particles are quite hard and during the ultramicrotoming process were evidently pulled out leaving behind voids, which appear as white features in the images. At the outset, TEM shows that MoS_2 layers are predominately located in polymer-swollen tactoids, mostly tens of nm in size, with much fewer larger scale tactoids (hundreds of nm in size). These tactoids are well dispersed throughout the polymer matrix (Fig. 3a and b). At higher magnifications, and focusing within and at the edges of the tactoids, TEM images reveal a good dispersion at the nanometer scale. For

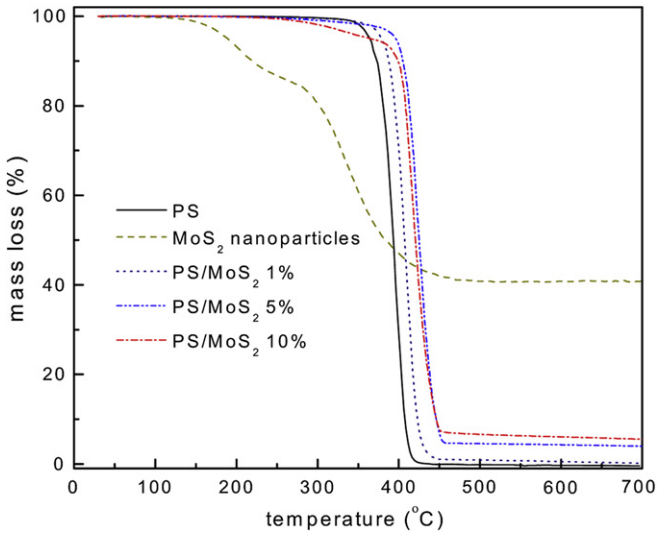

Fig. 5. TGA curves of neat PS and PS/MoS_2 nanocomposites with different MoS_2 content.

Table 1
Temperatures corresponding to characteristic mass losses of investigated samples.

Sample	10% wt loss temperature (°C)	50% wt loss temperature (°C)
PS	373	393
PS/MoS_2 1%	388	408
PS/MoS_2 5%	405	426
PS/MoS_2 10%	399	421
PMMA	240	345
PMMA/MoS_2 10%	325	366

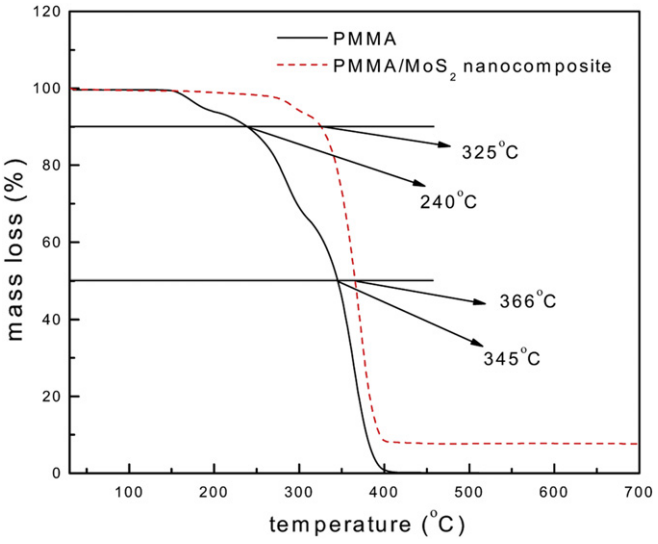

Fig. 6. TGA curves of neat PMMA and PMMA/MoS_2 nanocomposites with 10% of MoS_2 content.

example, nicely dispersed individual layers can be seen as dark lines at high magnifications in Fig. 3c, separated by polymer matrix regions (lighter gray features).

Similarly, TEM images obtained for PMMA/MoS_2 nanocomposites are shown in Fig. 4. These samples were more difficult to microtome due to cracking and fracture and only thick (>100 nm thick) sections could be obtained. As a result, in the high magnification images, Fig. 4b, it is not easy to resolve individual MoS_2 layers. Nonetheless, from the lower and medium magnification images, the dispersion of MoS_2 in PMMA appears to be similar to that in PS. Both systems can be described as nanocomposites with fillers well-dispersed at the nanometer scale – individual MoS2 layers – which are predominately located in tactoids that are tens of nm in size, whereas there also exist fewer larger, submicron-sized, filler clusters, *i.e.*, some conventional composite structure.

Fig. 5 depicts TGA curves of neat PS, MoS_2 and PS/MoS_2 nanocomposites with different MoS_2 content. The first degradation step of PS/MoS_2 nanocomposites starts at 270 °C, accompanied by the mass loss of about 5% in the nanocomposite with 10% MoS_2 while systems with a lower content of MoS_2 exhibit mass loss of less than 1%. This step is recognizable in the TGA-curve of pure filler, and is missing completely in the neat PS sample. This is likely due to the loss of the coordinating solvent from the MoS_2. The thermal decomposition of pure PS occurs in the range of 340–420 °C. The main degradation step of PS/MoS_2 nanocomposites follows very much the curve of pure PS. However, the thermal stability of the PS/MoS_2 nanocomposites is enhanced compared with that of the neat PS, which can be ascribed to the effect of MoS_2 on the diffusion of volatile products throughout the composite materials. The onset of the main thermal decomposition step of the nanocomposite with 5% MoS_2 content is shifted to 410 °C, which is approximately 20 °C higher in comparison to neat PS. When 50% mass loss point is selected as a point of comparison, the thermal decomposition temperatures for pure PS and PS/MoS_2 nanocomposites samples containing 1, 5 and 10% of the MoS_2 are found at 408, 426 and 421 °C, respectively; the results are shown in Table 1. The improvement is observable in the nanocomposite sample with as little as 1% MoS_2, and the effect is, of course, much more pronounced in samples with 5 or 10% MoS_2 content.

MoS_2 is also effective for promoting thermal stability in PMMA matrix. Fig. 6 shows TGA results for neat PMMA and PMMA/MoS_2 nanocomposite at 10% MoS_2 content. The degradation of neat PMMA occurs in three steps and PMMA nanocomposites in two steps, respectively, which is consistent with previous studies [15]. MoS_2 causes thermal stabilization of the PMMA which can be seen from the onset of the first thermal decomposition step, 85 °C higher for the nanocomposite with 10% MoS_2 compared to neat PMMA, and the temperature at which 50% degradation occurs, 21 °C higher. Essentially, the first step in the degradation, usually ascribed to the degradation of head-to-head linkages [21], is lost in the presence of MoS_2. This has also been seen when MMT is the nano-dimensional material [15].

Cone calorimetry is one of the most effective methods for the laboratory evaluation of the fire properties of polymers. The most important parameter is the heat release rate, HRR, and in particular its peak value PHRR. The reduction in PHRR is important for fire safety, as PHRR represents the point in a fire where heat is likely to propagate further, or ignite adjacent objects [22]. PHRR is usually significantly decreased for nanocomposites but depends upon particular polymer under investigation and not on the intercalated or exfoliated nature of the system [23]. In general, time to ignition is usually lower for nanocomposites, and the amount of smoke is about the same or a little bit larger while the mass loss rate is decreased. Table 2 presents the cone calorimetry data obtained at a heat flux of 50 kWm^{-2} for PS and its nanocomposite. The PHRR is reduced with an increase in the MoS_2 loading and the largest reduction in PHRR is noted for the sample with 10% MoS_2 loading. Consequently, the increase of MoS_2 loading decreases the average mass loss rate. Total heat release is slightly decreased in nanocomposites with 5 and 10%, respectively, and in the nanocomposite with 1% of MoS_2 content it remains the same. The time to sustained

Table 2
Cone calorimetry results for investigated samples at a heat flux of 50 kWm^{-2}.

Sample	PHRR[a] (kWm^{-2})	Reduct[a] (%)	THR[a] (MJm^{-2})	ASEA[a] (m^2kg^{-1})	AMLR[a] ($gs^{-1}m^{-2}$)	t_{ig}[a] (s)	Time to PHRR[a] (s)
PS	1158 ± 87	N/A	91 ± 2	1260 ± 401	31.0 ± 2.6	30 ± 2.5	89 ± 8
PS/MoS_2 1%	1041	10	92	1057	28.0	20	104
PS/MoS_2 5%	950 ± 105	18	82 ± 5	1017 ± 353	25.9 ± 2.2	16	99 ± 2
PS/MoS_2 10%	736 ± 38	36	73 ± 4	1307 ± 79	20.0 ± 1.0	12 ± 1.0	113 ± 10
PMMA	817 ± 32	N/A	95 ± 24	154 ± 18	25.7 ± 2.1	15 ± 4.2	107 ± 2
PMMA/MoS_2 10%	619 ± 28	24	88 ± 21	311 ± 13	20.5 ± 0.7	18 ± 6.4	106 ± 14

[a] PHRR – peak heat release rate; reduct – $PHRR_{Polymer}$-$PHRR_{nano}$/$PHRR_{PS}$; THR – total heat released; ASEA – average specific extinction area – a measure of smoke; AMLR – average mass loss rate; t_{ig} – time to ignition.

ignition, t_{ign}, is significantly reduced upon addition of MoS_2. It is assumed that addition of MoS_2 increases viscosity of the neat PS thus reducing heat exchange between the sample surface exposed to the radiant source and the bulk of the sample. This would result in a rapid increase in the surface temperature of the sample, hence the time required for the sample to reach the pyrolysis temperature is significantly reduced [24].

PMMA/MoS_2 nanocomposite with 10% MoS_2 loading also showed reduction in PHRR as expected. However, the time of sustained ignition slightly increased, but this could be assigned to measurement error or to variance rather than some interesting perception. Other results are in accordance with expectations for nanocomposite materials and are given in Table 2. The reduction in the PHRR is comparable to what is observed for PS/MMT or PMMA/MMT nanocomposites at 3% MMT loading [15].

Dynamic mechanical analysis (DMA) is used to measure the response of material to a cyclic deformation. The three main properties typically determined are the storage modulus (E') corresponding to the elastic response to the deformation, the loss modulus (E) describing the plastic response to the deformation, and their ratio, tanδ. Upon measuring at varied temperature, these properties can be related to transitions involving polymer mobility or segmental dynamics within the sample, such as the glass transition.

When added to polymer matrices, nanoparticles are known to cause changes in the dynamic properties of pristine material. Since the storage modulus is mainly related to the structure network created between the nanoparticles and macromolecular chains, its increase should be recorded. Due to the polymer–filler interactions, the adsorption of the polymer chains on the filler surface reduces the mobility of the polymeric segments. This interfacial zone surrounding the nanoparticles has a higher modulus and, sometimes, a higher T_g. Fig. 7 shows that the introduction of MoS_2 nanoparticles enhances the stiffness of nanocomposites which can be seen by the shift of the storage modulus curves compared to the storage modulus of the unfilled polymer, for all temperatures lower than the polymer's softening point.

Fig. 8 shows the loss modulus of neat PS and PS/MoS_2 nanocomposites. A thermomechanical, apparent, T_g can be determined by the peak maximum in the loss modulus vs. temperature dependence. Usually, this apparent T_g of a polymer tends to increase with the addition of nanoparticles, due to attractive

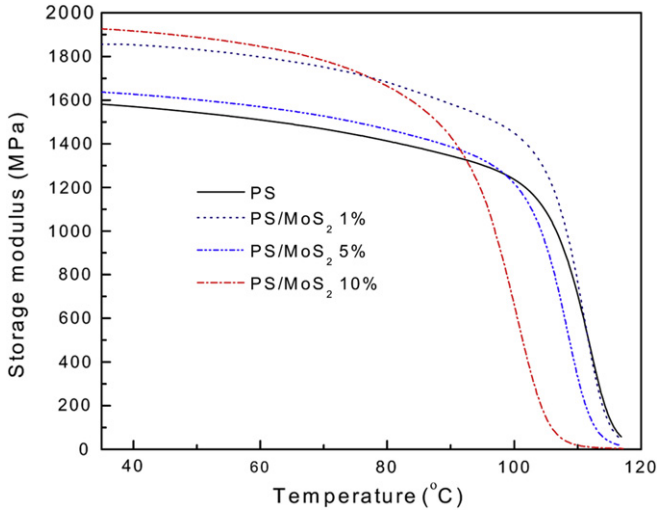

Fig. 7. Storage modulus of neat PS and PS/MoS_2 nanocomposites as a function of temperature.

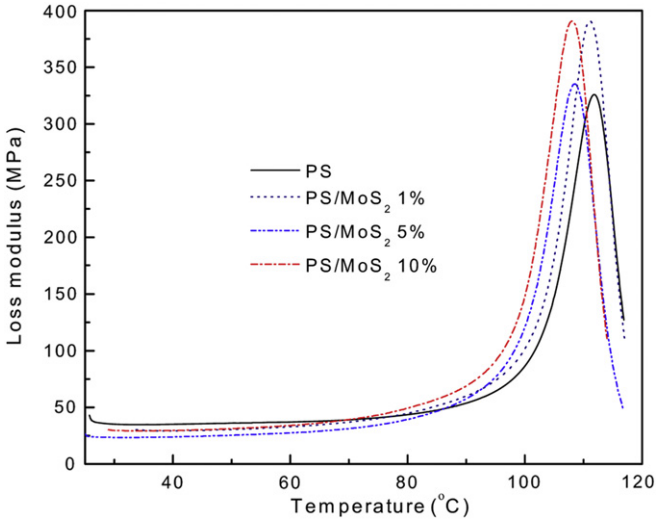

Fig. 8. Loss modulus of neat PS and PS/MoS_2 nanocomposite as a function of temperature.

Table 3
Tensile strength, elongation at break and Young's modulus of PS/MoS_2 nanocomposites as a ratio with unfilled PS.

Sample	Tensile strength, %	Elongation at break, %	Young's modulus, %
PS/MoS_2 1%	102	160	117
PS/MoS_2 5%	102	120	106
PS/MoS_2 10%	106	160	106

interactions between fillers and polymeric chains and due to the reduction of mobility at the interface around the nanoparticles. However, there are reports in the literature showing that this T_g can either remain unaffected by the addition of inorganic nanoparticles [25–27], or it may increase [28,29] or in some cases even decrease [30]. So, this effect is not consistent, but depends on the microstructure/amount of the nanoparticles, as well as on the interactions between the polymer and the filler [25,31]. In the case of PS/MoS_2 nanocomposites, it can be clearly seen that T_g remains almost unaffected by the addition of MoS_2.

An Instron test machine was used to measure the tensile strength and elongation at break for PS/MoS_2 nanocomposites. The results, as ratios against unfilled PS, are shown in Table 3. There is not much change for nanocomposites with different amount of MoS_2 nanoparticles added comparing to neat PS. The addition of MoS_2 to the PS matrix has a limited only effect on the mechanical properties of PS, in good agreement with the results from DMA.

DMA measurements and tensile tests were not performed for PMMA/MoS_2 nanocomposites due to the difficulties in preparing specimens.

4. Conclusions

MoS_2 nanoparticles with enhanced ability to disperse in polymeric matrices were successfully synthesized. PS and PMMA nanocomposites were prepared using a solution mixing technique. TEM results confirmed good nanometer-scale dispersion of MoS_2 in both PS and PMMA matrices with filler clustering in the sub-micron length scale, and both PS and PMMA nanocomposites showed enhanced thermal stability. For PS nanocomposites, the improvement in thermal stability was observable in the nanocomposite sample with as little as 1% MoS_2 and the effect was more pronounced in samples with 5 or 10% of MoS_2 content. PMMA nanocomposite showed great improvement in the first step of degradation, where

the onset temperature was almost 40 °C higher in comparison to neat PMMA, while the temperature at which 50% degradation occurs was 85 °C higher. Significant reductions in PHRR were also observed for all nanocomposites. Addition of MoS_2 nanoparticles enhanced the stiffness of PS/MoS_2 nanocomposites, which could be seen in the storage modulus at all temperatures lower than the polymer's softening point. At the same time, the glass transition temperatures remained largely unaffected upon addition of MoS_2. Tensile tests showed little change in strength or in elongation at break comparing PS/MoS_2 nanocomposites to the neat PS.

Acknowledgment

The work was financially supported by the US Air Force under grant number FA8650-07-1-5901 and by the US Department of Commerce, National Institute of Standards and Technologies, under grant number 70NANB10H224.

References

[1] Breysse M, Geantet C, Afanasiev P, Blanchard J, Vrinat M. Recent studies on the preparation, activation and design of active phases and supports of hydrotreating catalysts. Catal Today 2008;130:3–13.
[2] Dinter N, Rusanen M, Raybaud P, Kasztelan S, Silva PD, Toulhoat H. Temperature-programmed reduction of unpromoted MoS_2-based hydrodesulfurization catalysts: experiments and kinetic modeling from first principles. J Catal 2009;267:67–77.
[3] Yu L, Zhang P, Du Z. Tribological behaviour and structural change of the LB Film of MoS_2 nanoparticles coated with dialkyldithiphosphate. Surf Coat Technol 2000;130:110–5.
[4] Zhou X, Wu D, Shi H, Fu X, Hu Z, Wang X, et al. Study on tribological properties of surfactant-modified MoS_2 micrometer spheres as an additive in liquid paraffin. Tribol Int 2007;40:863–8.
[5] Rapoport L, Fleischer N, Tenne R. Applications of WS_2(MoS_2) inorganic nanotubes and fullerene-like nanoparticles for solid lubrification and for structural nanocomposites. J Mater Chem 2005;15:1782–8.
[6] Feng C, Ma J, Li H, Zeng R, Guo Z, Liu H. Synthesis of molybdenum disulfide (MoS_2) for lithium ion battery applications. Mater Res Bull 2009;44:1811–5.
[7] Xiao J, Choi D, Cosimbescu L, Koech F, Liu J, Lemmon JP. Exfoliated MoS_2 nanocomposite as an anode material for lithium ion batteries. Chem Mater 2010;22:4522–4.
[8] Benavente E, Santa Ana MA, Mendizábal F, González G. Intercalation chemistry of molybdenum disulfide. Coord Chem Rev 2002;24:87–109.
[9] Santa Ana MA, Mirabal N, Benavente E, Gómez-Romero P, González G. Electrochemical behaviour of lithium intercalated in a molybdenum disulfide-crown ether nanocomposite. Electrochim Acta 2007;53:1432–8.
[10] Shneider M, Dodiuk H, Kenig S, Tenne R. The effect of tungsten sulfide fullerene-like nanoparticles on the toughness of epoxy adhesives. J Adh Sci Tech 2009;23:753–68.
[11] Naffakh M, Marco C, Gomez MA, Jiminez I. Unique isothermal crystallization behavior of novel polyphenylene sulfide/inorganic fullerene-like WS2 nanocomposites. J Phys Chem B 2008;112:14819–28.
[12] Rapoport L, Nepomnyashchy O, Verdyan A, Popovitz R, Volonik Y, Ittah B, et al. Polymer nanocomposites with fullerene-like solid lubricant. Adv Eng Mater 2004;6:44–8.
[13] Hou X, Shan CX, Choy KL. Microstructures and tribological properties of PEEK-based nanocomposite coatings incorporating inorganic fullerene-like nanoparticles. Surf Coat Tech 2008;202:2287–91.
[14] Naffakh M, Martin Z, Fanegas N, Marco C, Gomez MA, Jiminez I. Influence of inorganic fullerene-like WS_2 nanoparticles on the thermal behavior of isotatic polypropylene. J Polym Sci Part B Polym Phys 2007;45:2309–21.
[15] Costache MC, Wang D, Heidecker MJ, Manias E, Wilkie CA. The thermal degradation of poly(methiyl methacrylate) nanocomposites with montmorillonite, layered double hydroxides and carbon nanotubes. Polym Adv Technol 2006;17:272–80.
[16] Yu H, Liu Y, Brock SL. Synthesis of discrete and dispersible MoS_2 nanocrystals. Inorg Chem 2008;47:1428–34.
[17] Zhou X. The study of restacked single molecular layer molybdenum disulfide with organic tetrachloroethylene Included. Master thesis; 2004.
[18] Joensen P, Frindt RF, Morrison SR. Single-layer MoS_2. Mater Res Bull 1986;21:457–61.
[19] Benavente E, González G. Microwave activated lithium intercalation in transition metal sulfides. Mater Res Bull 1997;32:709–17.
[20] Divigalpitiya WMR, Morrison SR, Frindt RF. Thin oriented films of molybdenum disulfide. Thin Solid Films 1990;186:177–92.
[21] Kashiwagi T, Inaba A, Brown JE, Hatada K, Kitayama T, Masuda E. Effect of weak linkages on the thermal and oxidative degradation of poly(methyl methacrylate). Macromol 1986;19:2160–8.
[22] Manzi-Nshuti C, Chen D, Su S, Wilkie CA. Structure-property relationships of new polystyrene nanocomposites prepared from initiator-containing layered double hydroxides of zinc aluminum and magnesium aluminum. Polym Degrad Sta 2009;94:1290–7.
[23] Wang D, Wilkie CA. *In situ* reactive blending to prepare polystyrene-clay and polypropylene-clay nanocomposites. Polym Degrad Stab 2009;94:770–81.
[24] Wang L, Su S, Chen D, Wilkie CA. Variation of anions in layered double hydroxides: effects on dispersion and fire properties. Polym Degrad Stab 2003;80:171–82.
[25] Vladimirov V, Betchev C, Vassiliou A, Papageorgiou G, Bikiaris D. Dynamic mechanical and morphological studies of isotactic polypropylene/fumed silica nanocomposites with enhanced gas barrier properties. Comp Sci Techn 2006;66:2935–44.
[26] Alexandre M, Dubois P. Polymer-layered silicate nanocomposites: preparation, properties and uses of a new class of materials. Mater Sci Eng 2000;28:1–63.
[27] Velasco JI, Ardanuy M, Realinho V, Antunes M, Fernández AI, González-Peña JI, et al. Polypropylene/clay nanocomposites: combined effects of clay compatibilizer polymers on the structure and properties. J Appl Polym Sci 2006;102:1213–23.
[28] Lu H, Xu X, Li X, Zhang Z. Morphology, crystallization and dynamic mechanical properties of PA66/nano-SiO_2 composites. Bull Mater Sci 2006;29:485–90.
[29] Lei SG, Hoa SV, Ton-That MT. Effect of clay type on the processing and properties of polypropylene nanocomposites. Com Sci Technol 2006;66:1274–9.
[30] Lin CH, Feng CC, Hwang TY. Preparation, thermal properties, morphology and microstructure of phosphorus containing epoxi/SiO_2 and polyimide/SiO_2. Eur Polym J 2007;43:725–42.
[31] Arabash A, Ahmad Z, AL-Sagheer F, Ali AAM. Microstructure and thermomechanical properties of polyimide-silica nanocomposites. J Nanomater 2006;1:1–9.